Temperature Sensing and Evaluation of Thermal Effects on Battery Packs for Automotive Applications

Temperature Sensing and Evaluation of Thermal Effects on Battery Packs for Automotive Applications

F. Ruffa, C. De Capua, *Member, IEEE*, R. Morello, Member*, IEEE*, Z. Liu, Senior *Member, IEEE*

***Abstract*—In this paper, we introduce the need for real-time temperature monitoring in battery packs used in automotive applications so to have an accurate estimation of battery life and performances. Advanced energy storage management systems should sense operating and ambient temperature of battery packs in order to implement proper strategies to improve the efficiency of charge and discharge processes and to extend battery life. The proposed evaluation technique is based on an innovative and dynamic circuital model, which allows to accurately represent the functioning of a battery pack (in charge and discharge) in the various operating conditions. Each circuital parameter of the model has a well-defined function which highlights its dependence on temperature, state of charge, state of health and number of cells. The model characterization has been made through tests on different battery sets. A climatic chamber has been used to simulate different operating conditions of ambient temperature. The analysis of the parameters evolution in time has led to the identification of an ideal ambient temperature range for the type of batteries under examination in order to improve their performances over time in terms of energy efficiency and extension of useful life.**

***Index Terms*—Circuital model, battery life estimation, battery performances, thermal effects, temperature sensing.**

I. Introduction

ENERGY storage systems are nowadays used in many applications ranging from high technology systems to consumer electronics and automotive applications. The increasing demand for smartphones, laptops, tablets has led to an increasing need for small and safe accumulators with a high energy density. For this reason, Lithium-ion batteries, which have a high energy density versus weight (140-180 Wh/kg) [1], have become a standard de facto for high technology. Lithium-ion batteries have even made possible the development of more features of the mobile devices and at the same time to reduce their dimension and weight. This has been essential also in automotive applications mainly for what concerns electric traction. As a consequence, today it is possible the project and development of more efficient energy storage systems.

Today more vehicles on the road are hybrid or (especially for public transport) purely electric. Furthermore, last regulations and directives for the environmental protection require a strong reduction in CO_2 emissions, like the European "*Clean Mobility Package*" target, which is intended to recommend a 30 % reduction of the average CO_2 emissions in 2030 compared to 2021. However, this is an unthinkable threshold to reach for a car with an internal combustion engine. For many of the applications mentioned above, and especially for automotive applications where performances, autonomy and cycle life are crucial, it is essential to know the current state of the battery so to exactly know what to expect from the battery in the present and future use, and then to implement efficient management systems [2]-[4]. Since accumulators are not ideal systems, their behavior and their characteristics change depending on the operating conditions and the current state. The most important indicators of the battery state are the *State of Charge* and *State of Health* (*SoC*, *SoH*). The first one is to indicate the amount of charge available in the battery, i.e. it is related to its capacity [5]; the last one is to indicate the actual capacity of the battery (in a specific moment of its life), i.e. it is related to the nominal capacity [6]. In literature, many mathematical and circuital models are used to statically and dynamically describe batteries or to determine their state during their functioning. Nevertheless, many of these models do not take into account how temperature affects the battery behavior in the various conditions of *SoC* and *SoH*. In this paper, we propose a new approach for the estimation of battery performances and cycle life. The proposed approach uses a circuital model, whose parameters are the functions of State of Charge and State of Health, the Temperature (*T*) and the number of battery cells. In this way, it is possible to exactly know what to expect from the battery in the various conditions of ambient and operating temperatures.

F.Ruffa, C. De Capua and R. Morello are with the Department of Information Engineering, Infrastructure and Sustainable Energy (DIIES), University Mediterranea of Reggio Calabria, Italy (e-mail: filippo.ruffa@unirc.it, claudio.decapua@unirc.it, rosario.morello@unirc.it).

Z. Liu is with the School of Engineering, the University of British Columbia Okanagan, Kelowna, BC, Canada (e-mail: zheng.liu@ubc.ca).

This is the post-print of the following article: F. Ruffa, C. De Capua, R. Morello and Z. Liu, "Temperature Sensing and Evaluation of Thermal Effects on Battery Packs for Automotive Applications," in IEEE Sensors Journal, vol. 19, no. 23, pp. 11634-11645, 1 Dec.1, 2019, doi: 10.1109/JSEN.2019.2933901. Article has been published in final form at: https://ieeexplore.ieee.org/document/8792106

II. STATE OF ART

It is well known from the literature that temperature affects the battery operations and life. In fact, battery manufacturers guarantee battery performances and cycle life in specific operating conditions and in a defined range of operating and storage temperature. Some of them provide also discharge curves at different temperature rates. However, temperature effects are still undervalued, in fact, modern battery management systems use temperature sensing mainly for safety purposes and not to implement better controls based on provisional data.

Battery Management Systems, in fact, are electronic circuits based on microcontroller systems used to monitor and control charge and discharge processes of battery packs and for charge balancing purposes. They implement a real-time monitoring of the single cell voltage, of the current rate and of battery pack temperature in order to control charge and discharge processes so to guarantee safety and battery life extension. It is possible to develop battery management systems that are able to take decisions based on provisional data provided by a model. However, the use of a complex model requires more computational capacity and memory, which means a higher cost of the hardware.

In literature, there are many models of electrochemical cells [7]. With the growth of batteries market, nowadays, many activities of research are focused on the optimization and discovery of new models. These are used in advanced battery management systems to implement effective run-time control and to provide provisional data on the future performances of the battery [8]-[11]. Electrochemical cell models are mainly of two types: mathematical [12], [13] and circuital-impedance based [14]. Some models are used for on-line estimation of the battery state [15]-[17] and are adapted to the specific operating conditions. In some recent solutions, charges and discharges are considered as stochastic and complex processes, and algorithms as Kalman Filter [18], [19], particle filter [20], [21] and others are used to simulate the batteries behaviour. Mathematical models are in general more accurate and can describe better even complex chemical processes than the circuital models; on the other hand, they have a higher computational complexity [22], [23].

For this reason, circuital models are well suited to be used in battery management systems. Circuital models use elements such as voltage sources, current sources and passive components to describe the behavior of a battery. As described in [24], Thevenin model [25] is the simplest one based on three elements: a voltage generator which represents the open circuit voltage (V_{oc}); a resistance R_0; and a R-C group to model the dynamic processes. This model assumes that the open-circuit voltage V_{oc} is constant. Unfortunately, this assumption prevents it from capturing steady-state battery voltage variations (i.e., DC response) as well as runtime information. Furthermore, one R-C group is not sufficient to accurately describe transients, which must be described by a higher order circuit. On the other hand, the more the R-C groups taken into account are, the more the model is accurate and complex. In order to have a good trade-off between accuracy and complexity, a good practice is to consider just two R-C groups [26] (see Figure 1 for reference). In this case, all parameters are function of *SoC*, *SoH* and *T*. Some advanced algorithms are used for the parameters identification, like genetic algorithms and frequency domain algorithms [27], [28].

Even though the circuital parameters of the model are strongly dependent on temperature, the works mentioned above do not analyse the dynamics of the parameters with temperature deeply. Differently, the analysis of such aspects would let the model get an overall characterization of the battery under test in various operating conditions.

The issue of the dynamics of the parameters depending on temperature has been analysed in some recent works, as in [29] and [30]. In [29] a dynamic Thevenin model is presented to evaluate the changes of the internal resistance with temperature; while in [30] it is demonstrated that an improved version of a Thevenin Model, whose parameters are determined in function of the ambient temperature, lets it have an higher accuracy in the description of the battery behavior in different operating conditions. In the present paper, we propose a global approach based on temperature monitoring which allows to have an accurate estimation of battery life and performances.

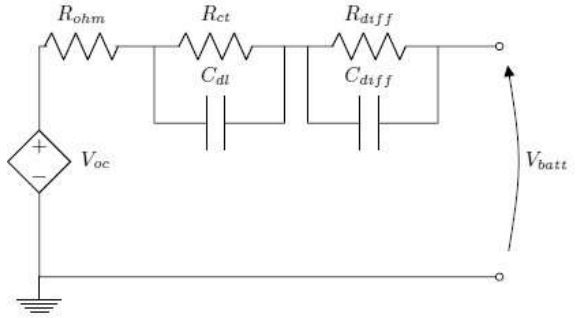

Fig. 1. Run- time Thevenin Model with two R-C groups.

III. METHODOLOGY

The models and algorithms above mentioned represent faithfully the discharge processes of energy storage systems during nominal operating conditions of ambient temperature. However, there are two open problems:

- they are not able to represent both the charge and discharge processes, this because the parameters trend in function of *SoC*, *SoH* and *T* is not the same for discharge and charge processes;
- the models and algorithms above mentioned, except [29] and [30], do not consider the dynamics of parameters as due to temperature variations.

The solution proposed in this paper is based on an innovative double R-C group with a directional circuital model, which can faithfully represent battery in both discharge and charge processes, using an improved version of the *Frequency Domain Identification Algorithm* (FDIA) [27], [28]. This algorithm allows to perform the identification of the circuit parameters and their dynamics characterization in function of *SoC*, *SoH* and *T*. The circuital model proposed is represented in Figure 2. All parameters are function of *SoC*, *SoH*, *T* and of the number *n* of cells of the battery.

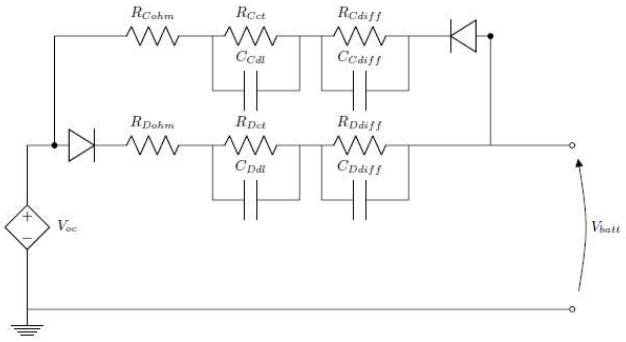

Fig. 2. Run-time directional circuital model with two R-C groups.

The considered parameters are: V_{oc}, which is the open circuit voltage at battery terminals in steady state condition; R_{Dohm} and R_{Cohm} which are to model contact and separator resistances in discharge and charge processes, respectively; R_{Dct}, C_{Ddl}, R_{Cct} and C_{Cdl} which are to model losses and dynamics due to the chemical reaction rate in discharge and charge processes, respectively; R_{Ddiff}, C_{Ddiff}, R_{Cdiff} and C_{Cdiff} which represent losses and dynamics due to charge diffusion in discharge and charge processes, respectively. Diodes are considered to be ideal, and their function is to fix the only available current direction across each branch of the circuit. V_{batt} is the voltage measured at battery terminals.

The impedance for each branch is:

$$\begin{cases} Z_D(j\omega) = \dfrac{\overline{V_{batt}}(j\omega) - \overline{V_{oc}}(j\omega)}{\overline{I_D}(j\omega)} \\ Z_C(j\omega) = \dfrac{\overline{V_{batt}}(j\omega) - \overline{V_{oc}}(j\omega)}{\overline{I_C}(j\omega)} \end{cases} \quad (1)$$

where:

$$\begin{cases} Z_D(j\omega) = \dfrac{\overline{V_{batt}}(j\omega) - \overline{V_{oc}}(j\omega)}{\overline{I_D}(j\omega)} = \left[R_{Dohm} + \dfrac{R_{Dct}}{1+s\tau_{Dct}} + \dfrac{R_{Ddiff}}{1+s\tau_{Ddiff}} \right]_{\substack{s=j\omega \\ SoC=SoC_i \\ T=T_i}} \\ Z_C(j\omega) = \dfrac{\overline{V_{batt}}(j\omega) - \overline{V_{oc}}(j\omega)}{\overline{I_C}(j\omega)} = \left[R_{Cohm} + \dfrac{R_{Cct}}{1+s\tau_{Cct}} + \dfrac{R_{Cdiff}}{1+s\tau_{Cdiff}} \right]_{\substack{s=j\omega \\ SoC=SoC_i \\ T=T_i}} \end{cases} \quad (2)$$

with $\tau_{Dct} = R_{Dct}C_{Ddl}$, $\tau_{Ddiff} = R_{Ddiff}C_{Ddiff}$, $\tau_{Cct} = R_{Cct}C_{Cdl}$ and $\tau_{Cdiff} = R_{Cdiff}C_{Cdiff}$.

Separating the real part from the imaginary part, it is possible to evaluate:

$$Z_D(j\omega) = \frac{a_D(\omega) + jb_D(\omega)}{d_D(\omega)}$$

$$\begin{cases} a_D(\omega) = \omega^2 \left(\omega^2 \tau_{Dct}^2 \tau_{Ddiff}^2 R_{Dohm} + \tau_{Dct}^2 (R_{Dohm} + R_{Ddiff}) + \tau_{Ddiff}^2 (R_{Dohm} + R_{Dct}) \right. \\ \qquad \left. + R_{Dohm} + R_{Dct} + R_{Ddiff} \right. \\ b_D(\omega) = -\omega \left(\tau_{Dct} R_{Dct} + \tau_{Ddiff} R_{Ddiff} + \omega^2 \tau_{Dct} \tau_{Ddiff} (\tau_{Dct} R_{Ddiff} + \tau_{Ddiff} R_{Dct}) \right) \\ d_D(\omega) = 1 + \omega^2 (\omega^2 \tau_{Dct}^2 \tau_{Ddiff}^2 + \tau_{Dct}^2 + \tau_{Ddiff}^2) \end{cases} \quad (3)$$

this is valid for the branch representing the discharge process, and:

$$Z_C(j\omega) = \frac{a_C(\omega) + jb_C(\omega)}{d_C(\omega)}$$

$$\begin{cases} a_C(\omega) = \omega^2 \left(\omega^2 \tau_{Cct}^2 \tau_{Cdiff}^2 R_{Cohm} + \tau_{Cct}^2 (R_{Cohm} + R_{Cdiff}) + \tau_{Cdiff}^2 (R_{Cohm} + R_{Cc} \right. \\ \qquad \left. + R_{Cohm} + R_{Cct} + R_{Cdiff} \right. \\ b_D(\omega) = -\omega \left(\tau_{Cct} R_{Cct} + \tau_{Cdiff} R_{Cdiff} + \omega^2 \tau_{Cct} \tau_{Cdiff} (\tau_{Cct} R_{Cdiff} + \tau_{Cdiff} R_{Cct}) \right) \\ d_D(\omega) = 1 + \omega^2 (\omega^2 \tau_{Cct}^2 \tau_{Cdiff}^2 + \tau_{Cct}^2 + \tau_{Cdiff}^2) \end{cases} \quad (4)$$

Which is valid for the branch representing the charge process.

If the temperature is known and constant, and even *SoH* is known, the identification algorithm works as follows:

1. *SoC* is measured with *Coulomb Counting Technique*, whose expression is reported in the following:

$$SoC(t) = SoC(t_0) - 100 \int_{t_0}^{t} \frac{i(\tau)}{C_{eff} * 3600} \mathrm{d}\tau ; \quad (5)$$

2. V_{oc} is measured in steady state condition, with $I_b=0$ and $\mathrm{d}V_m / \mathrm{d}t = 0$. This condition is reached when all dynamic effects due to long transients are exhausted. The time needed to complete transients depends on the specific battery technology and capacity. So the battery is kept in an idle state for a certain amount of time, after which, the voltage at battery terminals is almost constant and equal to the open circuit voltage. Indicating with t_0 the instant of time when the current flows through the battery is stopped, and with Δt^* the amount of time needed to exhaust transients, it is obtained:

$$V_{oc}(t_0 + \Delta t^*) \approx V_{batt}(t_0 + \Delta t^*)\,|_{SoC(t_0+\Delta t^*)=SoC(t_0)} \quad (6)$$

Using equation (6), the open circuit voltage is evaluated by measuring the voltage at battery terminals after a specified rest time;

3. the voltage drop across battery internal impedance is measured as:

$$V(t) = V_{oc}(t) - V_{batt}(t) ; \quad (7)$$

4. $V(t)$ and the battery current $I_{batt}(t)$ are evaluated in the frequency domain by a FFT transformer;
5. using equations (1), (2), (3) and (4), the cost functions for module and phase are evaluated as in the following for discharge and charge processes, respectively:

$$\begin{cases} F_{Dm}(\omega) = \dfrac{\sqrt{a_D(\omega)^2 + b_D(\omega)^2}}{d_D(\omega)} |I_D(\omega)| - |V(\omega)| \\ F_{Dp}(\omega) = \arctan\left(\dfrac{b_D(\omega)}{a_D(\omega)}\right) + \arg\left(I_D(\omega)\right) - \arg\left(V(\omega)\right) \end{cases} \quad (8)$$

$$\begin{cases} F_{Cm}(\omega) = \dfrac{\sqrt{a_C(\omega)^2 + b_C(\omega)^2}}{d_C(\omega)} |I_C(\omega)| - |V(\omega)| \\ F_{Cp}(\omega) = \arctan\left(\dfrac{b_C(\omega)}{a_C(\omega)}\right) + \arg\left(I_C(\omega)\right) - \arg\left(V(\omega)\right) \end{cases} \quad (9)$$

The cost functions in (8) and (9) are simplified by using the *Least Squares Optimization Technique*. The result gives an estimation of the unknown parameters for each branch of the circuital model. In this way, by repeating the previous steps in different operating conditions of the ambient temperature, we have a set of points for each parameter. To interpolate the sampled points, a *polynomial fitting* function has been used. In this way, it has been possible to obtain a math relation for each parameter which is function of *SoC*, *SoH*, *T* and of the number *n* of cells of the battery:

$$\begin{aligned}
V_{oc}(SoC,SoH,T,n) &= \sum_{i=0}^{m}\sum_{j=0}^{m} v_{ij}(SoH,n) * SoC^i * T^j \\
R_{Dohm}(SoC,SoH,T,n) &= \sum_{i=0}^{m}\sum_{j=0}^{m} a_{Dij}(SoH,n) * SoC^i * T^j \\
R_{Cohm}(SoC,SoH,T,n) &= \sum_{i=0}^{m}\sum_{j=0}^{m} a_{Cij}(SoH,n) * SoC^i * T^j \\
R_{Dct}(SoC,SoH,T,n) &= \sum_{i=0}^{m}\sum_{j=0}^{m} b_{Dij}(SoH,n) * SoC^i * T^j \\
R_{Cct}(SoC,SoH,T,n) &= \sum_{i=0}^{m}\sum_{j=0}^{m} b_{Cij}(SoH,n) * SoC^i * T^j \\
C_{Ddl}(SoC,SoH,T,n) &= \sum_{i=0}^{m}\sum_{j=0}^{m} c_{Dij}(SoH,n) * SoC^i * T^j \\
C_{Cdl}(SoC,SoH,T,n) &= \sum_{i=0}^{m}\sum_{j=0}^{m} c_{Cij}(SoH,n) * SoC^i * T^j \\
R_{Ddiff}(SoC,SoH,T,n) &= \sum_{i=0}^{m}\sum_{j=0}^{m} d_{Dij}(SoH,n) * SoC^i * T^j \\
R_{Cdiff}(SoC,SoH,T,n) &= \sum_{i=0}^{m}\sum_{j=0}^{m} d_{Cij}(SoH,n) * SoC^i * T^j \\
C_{Ddiff}(SoC,SoH,T,n) &= \sum_{i=0}^{m}\sum_{j=0}^{m} e_{Dij}(SoH,n) * SoC^i * T^j \\
C_{Cdiff}(SoC,SoH,T,n) &= \sum_{i=0}^{m}\sum_{j=0}^{m} e_{Cij}(SoH,n) * SoC^i * T^j
\end{aligned} \quad (10)$$

where the values v_{ij}, a_{Dij}, a_{Cij}, b_{Dij}, b_{Cij}, c_{Dij}, c_{Cij}, d_{Dij}, d_{Cij}, e_{Dij} and e_{Cij} are experimentally evaluated and are function of the number *n* of cells and of *SoH*.

The computational complexity of the overall procedure has been calculated by analysing the computational complexity of each single step of the algorithm, as in the following:

- *FFT* transformer, complexity $O(NlogN)$;
- *Least Squares Technique*, complexity $O(C^2N)$;
- *Polynomial Fitting Technique* $O(K^2)$;

where N is the number of samples of a discharge/charge process, C represents the circuital parameters and K represents the number of points measured for each parameter with the procedure described above. Consequently, the total computational complexity is $O(C^2N)$.

IV. MEASUREMENT SETUP

Once the model has been defined, it has been validated on a set of cells. Experimental data have been collected by carrying out several tests. To do that, an automated experimental platform has been built, it is able to monitor and control current discharge and standard charge processes for lead acid, Nickel based and Lithium ion batteries. Furthermore, the developed platform can perform discharge and charge processes with pulsed current profiles. It consists of a fast switching power supply, a programmable fast switching electronic load, a power analyser, two acquisition modules, current and temperature transducers. All the instruments are connected through a communication bus to an *Energy Storage Management System* implemented in *NI LabVIEW* environment, which has the task to monitor and control charge and discharge processes.

The automated platform, whose configuration is showed in Figures 3 and 4, consists of the following instrumentation:

- Power Supply *Ametek SGI 15/801*;
- Programmable Electronic Load *Amrel PLA 10K-60-1500*;
- Power Analyser *Yokogawa WT1800*;
- Data Acquisition Switch *Agilent 34970A* (for temperature measurements);
- *NI CompactDAQ* with the acquisition module *NI9233*;
- a Type *J thermocouple*;
- a current transducer *LEM CT 10-T*;
- Climatic Chamber *Angelantoni Discovery DY250*.

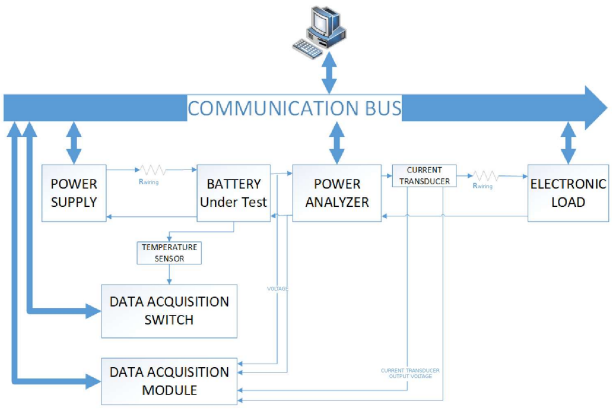

Fig. 3. Experimental platform architecture.

Fig. 4. Experimental platform instrumentation.

The power supply has to feed current to the battery during the charge process, differently it works in open circuit mode during the discharge process. On the other hand, the *Programmable Electronic Load* has the task to absorb current from the battery during the discharge process. The *Power Analyser* monitors the following parameters with a sampling frequency of 20 S/s:

- Current [A];
- Battery voltage [V];
- Single cell voltage [V];
- Charge [Ah];
- Instantaneous power [W];
- Energy [Wh].

The *Data Acquisition Switch* with a *Type-J thermocouple* has the task to monitor the temperature T [°C] of the cell with a sampling frequency of 20 S/s.

During the transients due to pulsed and fast switching in the charge and discharge processes, some parameters (Current [A], Battery voltage [V], Single cell voltage [V]) are monitored with the *NI-CompactDAQ* and the acquisition module *NI9233* at a sampling rate of 2 kS/s so to get information on fast changes.

The *current transducer* is used to convert the current in voltage signal with a sensibility of 10A/5V so to be sampled by the *NI9233* module.

The *Climatic Chamber* has been used to simulate different working conditions by changing and maintaining constant the ambient temperature in which the batteries operate. Three target temperatures have been considered for the characterization of the batteries under test: 0 °C, 25 °C and 50 °C.

Since the final aim of the present study is to evaluate the thermal effects on batteries used in electric traction, the proposed model has been applied to test $LiFePO_4$ accumulators. This accumulator technology is today widely used in electric vehicles. The units under test consist of scaled accumulators based on two 3.2 V 2300 mAh $LiFePO_4$ cells displaced in series configuration. The single cell is shown in Figure 5.

Fig. 5. The 2300mAh $LiFePO_4$ cell under test.

The used test profiles have been designed to excite the resistive-capacitive behavior of the battery. The methodology described in the previous Section has been used to evaluate the parameters of the circuital model and their evolution over time.

All tests have been executed in the *Climatic Chamber* at different temperature set points so to characterize the temperature effects on battery performances and life. The following procedure has been used for each single set of batteries:

1. the ambient temperature in the climatic chamber is set at the target temperature;
2. pre-charge of the single cell: each cell is fully charged before to connect the cells in series to avoid charge unbalances;
3. perform 4 settling discharge and charge cycles: this step does not require a deep discharge cycle, the battery is discharged down to a 20% of *SoC* and then re-charged;
4. the ambient temperature in the climatic chamber is keep at target temperature for at least two hours before to start the parametric test;
5. Parametric Test: a full discharge cycle is executed and followed by a full charge cycle. All discharge cycles are Constant Current Discharge with a current rate of 1C. The charge cycles are Standard Li-Ion Charge Cycle at a current of 0.5C. The initial capacity is measured with the Coulomb Counting Technique. *SoH* is assumed to be 100%;
6. the climatic chamber is set to maintain the target temperature constant during the test and for two hours before to start the test operations;
7. Pulsed Discharge Profile: the battery is fully discharged with a 2C current pulse train. Each current pulse extracts from battery a 10% of charge and it is followed by a rest time of 1800 s after which V_{oc} is measured. Figure 6 shows the used current discharge profile;

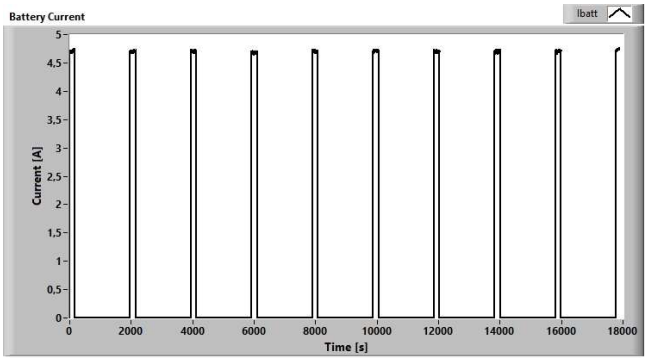

Fig. 6. Current Discharge Profile.

8. Pulsed Charge Profile: the battery is fully charged by using a 0.5C current pulse train. Each current pulse feeds to battery a 10% charge level and it is followed by a rest time of 1800s after which V_{oc} is measured. Figure 7 shows the used current charge profile.
9.

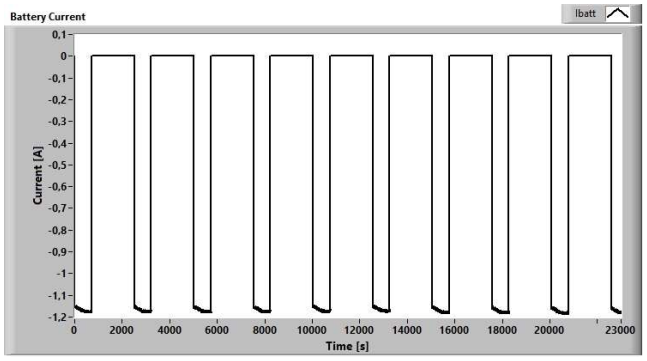

Fig. 7. Current Charge profile.

10. A topping charge (Standard charge) is performed in order to complete the charge operation by using a constant voltage stage;
11. Points from 7 to 9 are repeated for 10 times;
12. The ambient temperature in the climatic chamber is maintained still at the target temperature and the battery is let at rest for two hours before starting the parametric test;
13. Parametric Test: a full discharge cycle is executed and followed by a full charge cycle. All discharge cycles are Constant Current Discharge cycle at a current rate of 1C. The charge cycles are Standard Li-Ion Charge Cycle at a current of 0.5 C. The residual capacity with the Coulomb Counting Technique is measured and the battery SoH is evaluated by the equation $SoH = 100\ C_t/C_{nom}$;
14. Points from 6 to 12 are repeated 3 times.

The above described test procedure has been carried out on three different sets of new batteries. Three target temperatures have been chosen: 0 °C, 25 °C and 50 °C. The final aim of the performed tests was to obtain information about the battery run-time behavior and its lifetime evolution in different operating conditions of the ambient temperature. Data obtained from the tests have been processed with the algorithm described in Section III and the obtained results are shown in Section V.

V. RESULTS

The experimental results have allowed us to characterize the resistive-capacitive model of the battery in function of its *State of Charge*, *State of Health* and *Temperature* in order to evaluate the temperature impact on the battery performances and life.

For what concerns internal resistances R_{Dohm} and R_{Cohm}, the values experimentally measured include the contribution of the contact resistance due to the electrical contacts. The contact resistance $R_{contact}$ was measured at each target temperature with the *Fall of Potential Method*, so obtaining:

$$R_{contact} = \begin{cases} 0.0230\Omega & T = 0^{\circ}C \\ 0.0190\Omega & T = 25^{\circ}C \\ 0.0165\Omega & T = 50^{\circ}C \end{cases} \quad (11)$$

The $R_{contact}$ value has been subtracted from the measured data points in order to evaluate the correct values of R_{Dohm} and R_{Cohm}, so improving the accuracy of the functions of all considered parameters. In detail, to show the experimental results, for each considered parameter, the respective equation and graph are reported in the following.

The equation and graphical representation of the V_{oc} function are reported below by considering its dependence from T and SoC with SoH=100%, respectively in (12) and in Figure 8:

$$V_{oc}(SoC, SoH, T, n) = \sum_{i=0}^{m}\sum_{j=0}^{m} v_{ij}(SoH, n) * SoC^{i} * T^{j} \quad (12)$$

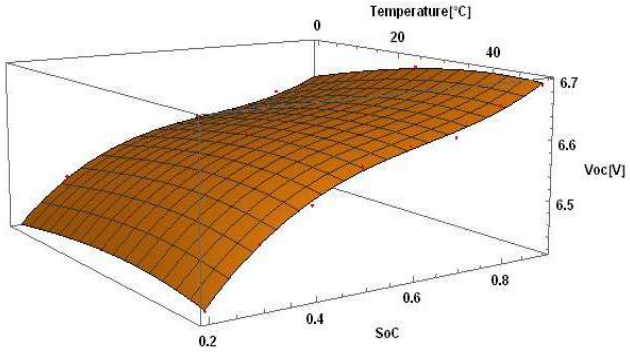

Fig. 8. V_{OC} trend in function of SoC and T.

Figure 8 shows how the open circuit voltage depends on the *State of Charge* and *Temperature*. In fact, V_{oc} increases as the SoC increases, but it has also a strong dependence on T. In detail, by keeping SoC constant, V_{oc} increases with T getting a maximum value between 30 °C and 40 °C. This depends on the battery SoC.

The equation and graphical representation of the R_{Dohm} function are reported in (13) and in Figure 9, respectively:

$$R_{Dohm}(SoC, SoH, T, n) = \sum_{i=0}^{m}\sum_{j=0}^{m} a_{Dij}(SoH, n) * SoC^{i} * T^{j} \quad (13)$$

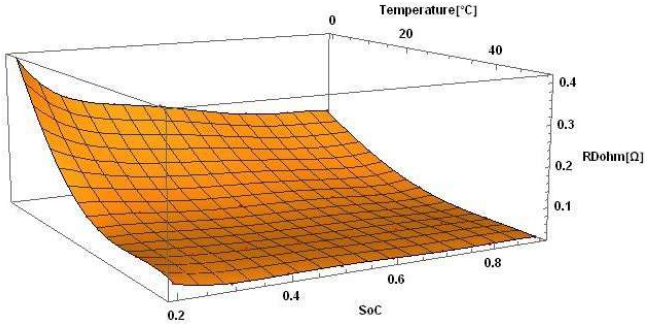

Fig. 9. R_{Dohm} trend in function of SoC and T.

In detail, Figure 9 shows how the internal resistance in the discharge branch depends graphically on *SoC* and *T*. Higher internal resistance values are cause of greater losses, consequently it involves a lower efficiency in transferring charge. R_{Dohm} is lower when the battery has full-charge and increases as the battery is discharged and the *SoC* decreases. This parameter has also a strong dependence on temperature, in particular it increases as temperature decreases, which means that the battery does not operate well at low temperatures.

The equation of the R_{Dct} function is reported in (14):

$$R_{Dct}(SoC, SoH, T, n) = \begin{cases} \sum_{i=0}^{m}\sum_{j=0}^{m} b_{1\,Dij}(SoH, n) * SoC^{i} * T^{j} & SoC < 0.4 \\ \sum_{i=0}^{m}\sum_{j=0}^{m} b_{2\,Dij}(SoH, n) * SoC^{i} * T^{j} & 0.4 < SoC < 0.7 \\ \sum_{i=0}^{m}\sum_{j=0}^{m} b_{3\,Dij}(SoH, n) * SoC^{i} * T^{j} & SoC > 0.7 \end{cases} \quad (14)$$

Because of the discontinuous trend of data points, the best fit result has been obtained by cutting this function in three parts determined by three different ranges of *SoC*.

This resistance describes the losses due to the battery electrochemical reaction. The minimum values have been got in the *SoC* range from 50% to 80%. Then it increases as the battery is discharged and the *SoC* decreases.

The equation and graphical representation of the C_{Ddl} function are reported in (15) and in Figure 10, respectively:

$$C_{Ddl}(SoC, SoH, T, n) = \sum_{i=0}^{m}\sum_{j=0}^{m} c_{Dij}(SoH, n) * SoC^{i} * T^{j} \quad (15)$$

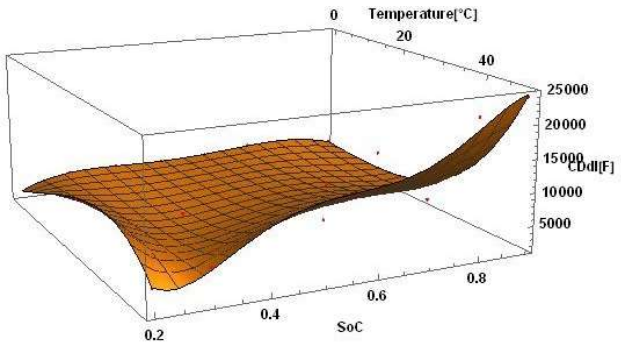

Fig. 10. C_{Ddl} trend in function of SoC and T.

Figure 10 shows how the double-layer capacitance in the discharge branch depends on *SoC* and *T*. This parameter and R_{Dct} allow us to model the dynamics due to the battery chemical reaction. In particular, C_{Ddl} does not vary significantly with *SoC* except at high temperatures. As a consequence, during a discharge process, there are not huge variations in C_{Ddl} value. Differently, it has a significant dependence on *T*, so C_{Ddl} increases with *T* and, at high temperatures, it decreases while the battery is discharged. This means that the dynamic due to the chemical reaction is slower at high temperatures.

The equation and graphical representation of the R_{Ddiff} function are reported in (16) and in Figure 11, respectively:

$$R_{Ddiff}(SoC, SoH, T, n) = \sum_{i=0}^{m}\sum_{j=0}^{m} d_{Dij}(SoH, n) * SoC^{i} * T^{j} \quad (16)$$

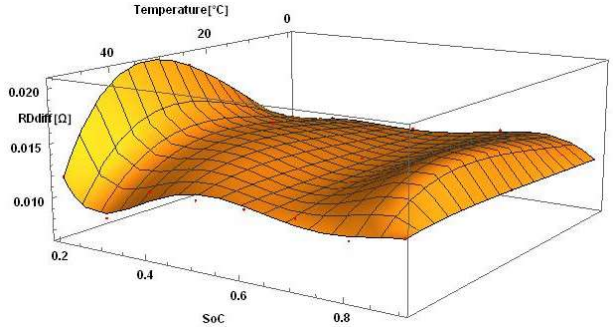

Fig. 11. R_{Ddiff} trend in function of SoC and T.

Figure 11 shows how the diffusion resistance in the discharge branch depends on *SoC* and *T*. This resistance describes the losses due to the diffusion of carriers. R_{Ddiff} is higher at higher temperatures and does not vary significantly during the discharge process, except near to the end of the discharge condition.

The equation and graphical representation of the C_{Ddiff} function are reported in (17) and in Figure 12, respectively:

$$C_{Ddiff}(SoC, SoH, T, n) = \sum_{i=0}^{m}\sum_{j=0}^{m} e_{Dij}(SoH, n) * SoC^{i} * T^{j} \quad (17)$$

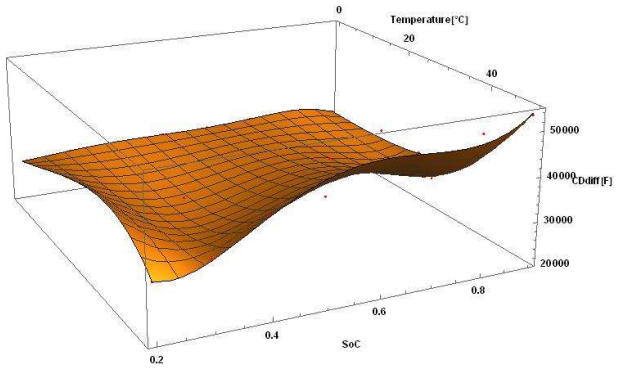

Fig. 12. C_{Ddiff} trend in function of SoC and T.

Figure 12 shows how the diffusion capacitance in the discharge branch depends on *SoC* and *T*. This parameter and

R_{Ddiff} allow us to characterize the dynamics due to the diffusion of carriers, in this case the diffusion process is slower than that due to the chemical reaction. C_{Ddiff} (as C_{Ddl}) does not vary significantly with *SoC* except at high temperatures. As a consequence, during a discharge process, there are not huge variations in C_{Ddiff} value. Differently, it has a significant dependence on *T*, so C_{Ddiff} increases with temperature and, at high temperatures, it decreases while the battery is discharged. This means that the dynamics due to the diffusion of carriers are slower at high temperatures.

The equation and graphical representation of the R_{Cohm} function are reported in (18) and in Figure 13, respectively:

$$R_{Cohm}(SoC, SoH, T, n) = \sum_{i=0}^{m}\sum_{j=0}^{m} a_{Cij}(SoH, n) * SoC^{i} * T^{j} \quad (18)$$

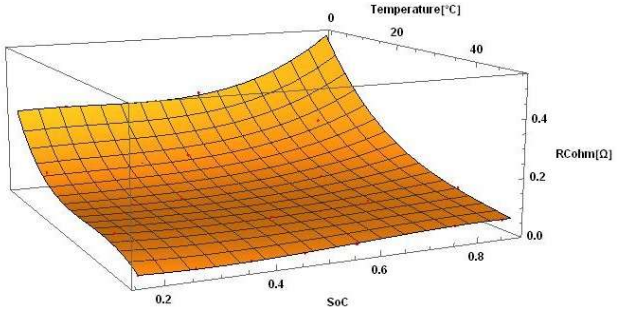

Fig. 13. R_{Cohm} trend in function of SoC and T.

Figure 13 shows how the internal resistance in the charging branch depends on *SoC* and *T*. Higher internal resistance values are cause of greater losses with a lower efficiency of the charging process. Differently from what happens on the discharge branch, R_{Cohm} is lower when the battery is empty and increases as the battery is charged and the *SoC* value increases. The curve slope becomes greater at the end of the charge condition, i.e. when the battery begins to refuse further charge. This parameter has a strong dependence on *T*, so both R_{Cohm} and R_{Dohm} increase as temperature decreases, which means that the battery does not operate well at low temperatures.

The equation and graphical representation of the R_{Cct} function are reported in (19) and in Figure 14, respectively:

$$R_{Cct}(SoC, SoH, T, n) = \sum_{i=0}^{m}\sum_{j=0}^{m} b_{Cij}(SoH, n) * SoC^{i} * T^{j} \quad (19)$$

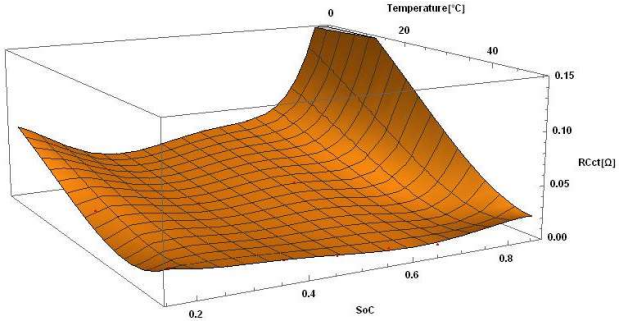

Fig. 14. R_{Cct} trend in function of SoC and T.

Figure 14 shows how the charge transfer resistance in the charging branch depends on *SoC* and *T*. R_{Cct} describes the losses due to the battery electrochemical reaction during the charge process. The minimum values have been got in the *SoC* range from 20% to 40%. Then it increases as the battery is charged and the *SoC* increases. Similarly to R_{Cohm}, R_{Cct} is higher at low temperatures.

The equation of the C_{Cdl} function is reported in (20):

$$C_{Cdl}(SoC, SoH, T, n) = \begin{cases} \sum_{i=0}^{m}\sum_{j=0}^{m} c_{1Cij}(SoH, n) * SoC^{i} * T^{j} & SoC \le 0.48 \\ \sum_{i=0}^{m}\sum_{j=0}^{m} c_{2Cij}(SoH, n) * SoC^{i} * T^{j} & 0.48 < SoC < 0.68 \\ \sum_{i=0}^{m}\sum_{j=0}^{m} c_{3Cij}(SoH, n) * SoC^{i} * T^{j} & SoC \ge 0.68 \end{cases} \quad (20)$$

Because of the discontinuous trend of data points, the best fit result has been obtained by cutting this function in three parts determined by three different ranges of *SoC*. This parameter and R_{Cct} allow us to model the dynamics due to the battery chemical reaction during the charge process. C_{Cdl} is higher at high temperatures.

The equation and graphical representation of the R_{Cdiff} function are reported in (21) and in Figure 15, respectively:

$$R_{Cdiff}(SoC, SoH, T, n) = \sum_{i=0}^{m}\sum_{j=0}^{m} d_{Cij}(SoH, n) * SoC^{i} * T^{j} \quad (21)$$

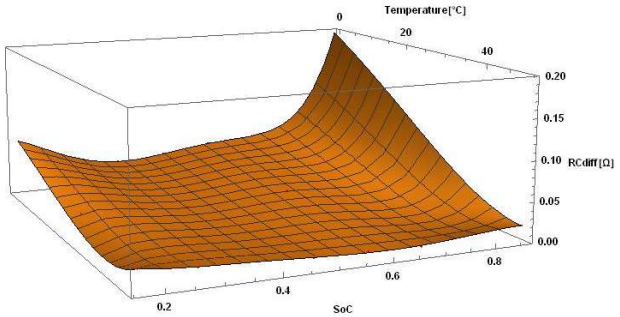

Fig. 15. R_{Cdiff} trend in function of SoC and T.

Figure 15 shows how the diffusion resistance in the charging branch depends on *SoC* and *T*. R_{Cdiff} represents the losses due to carriers diffusion during the charge process. The minimum values have been got in *SoC* range from 20% to 40%. Then it increases as the battery is charged and the *SoC* increases. Similarly to R_{Cohm} and R_{Cct}, R_{Cdiff} is higher at low temperatures. The equation of the C_{Cdiff} function is reported in (22):

$$C_{Cdiff}(SoC, SoH, T, n) = \begin{cases} \sum_{i=0}^{m}\sum_{j=0}^{m} e_{1Cij}(SoH, n) * SoC^{i} * T^{j} & SoC \le 0.48 \\ \sum_{i=0}^{m}\sum_{j=0}^{m} e_{2Cij}(SoH, n) * SoC^{i} * T^{j} & 0.48 < SoC < 0.58 \\ \sum_{i=0}^{m}\sum_{j=0}^{m} e_{3Cij}(SoH, n) * SoC^{i} * T^{j} & SoC \ge 0.58 \end{cases} \quad (22)$$

Because of the discontinuous trend of data points, the best fit result has been obtained by cutting this function in three parts determined by three different ranges of *SoC*. This parameter and R_{Cdiff} allow us to model the dynamics due to carriers diffusion during the charge process, this diffusion is slower than that due to the battery chemical reaction.

The above 3D functions have been computed by using the polynomial fitting technique between known points of the software *Wolfram Mathematica*. The sets of data points refer to the tests carried out at the target temperature values 0 °C, 25 °C and 50 °C with ΔSoC intervals of 0.1.

The conclusion of this experimentation was that the battery set which has been tested at 50 °C has lost much more capacity then the batteries tested at 0 °C and 25 °C. The capacity was measured with the *Coulomb Counting technique* during the parametric tests. Table I reports the available capacity at the end of the experimentation for each unit under test.

TABLE I
RESIDUAL CAPACITY AND SOH AT THE END OF TEST OPERATIONS

	Starting Capacity [Ah]	Final Capacity [Ah]	SoH [%]
0°C	2.22	2.13	96
25°C	2.22	2.175	98
50°C	2.22	2.05	93

Further analysis comes from the characterization of the proposed model. By considering the model and analysing the values of each parameter cycle by cycle, it is possible to obtain a curve which describes the evolution of the single parameter in function of the number of cycles and of the temperature. The reference parameter to evaluate the battery ageing is the internal resistance R_{Dohm} in the discharge branch. From literature, an increment of the internal resistance in the same operating conditions and at the same *State of Charge* can be directly related to a reduction of the battery *State of Health*. Figure 16 shows the R_{Dohm} curve at *SoC*=90% in function of the number of cycles and of the temperature.

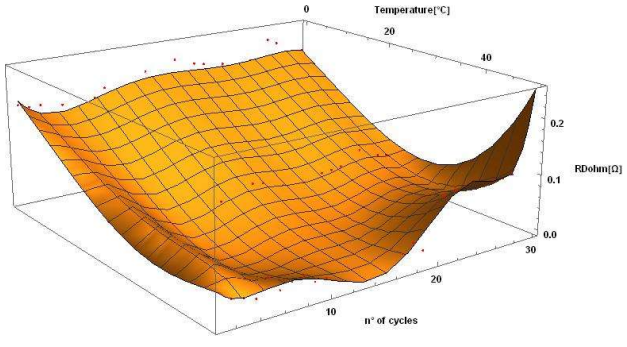

Fig. 16. R_{Dohm} evolution in function of the number of cycles and T at SoC=0.9.

The curve is obtained with the polynomial fitting technique, and the data points are depicted by red dots. Figure 17 shows the partial derivative $\partial R_{Dohm} / \partial n$ function. It provides significant information on how the variation of R_{Dohm} is fast in the different operating conditions.

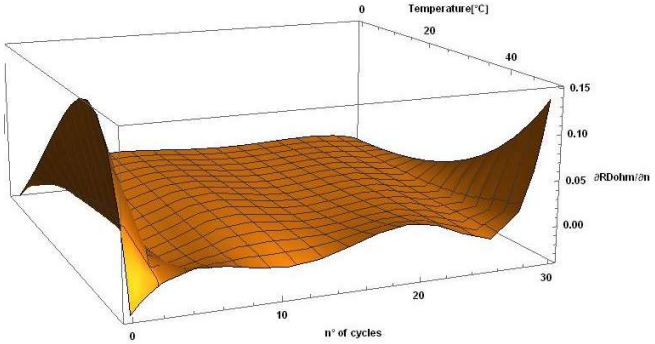

Fig. 17. Partial derivative $\partial R_{Dohm} / \partial n$ of the function reported in Figure 16.

It is interesting to note that for all operating conditions the function $\partial R_{Dohm} / \partial n$ has a negative trend in the first 3-5 cycles, i.e. the internal resistance decreases in the starting cycles. Then it reaches its final value. This behaviour is because a new battery needs some training charge/discharge cycles in order to reach its maximum performances. Then the internal resistance increases as battery ages. The curve, obtained by interpolating the experimental data, highlights that the internal resistance does not vary significantly at low and mid temperatures in the first 30 cycles.

The graph of the resistance R_{Dohm} has its maximum values at 0°C. Then it decreases with the increase of the temperature, obtaining the minimum value of the internal resistance at 50 °C. However, if in the range of temperature from 0 °C to 30°C the internal resistance does not vary significantly in the first 30 cycles, this is not true at higher temperatures. In fact, the higher is temperature the faster internal resistance increases over time. It is important to note that high values of internal resistance mean high losses, consequently this is indicative of a low energy efficiency during the discharge and charge processes. In addition, the battery reaches earlier the fully discharged and fully charged states, entailing as consequence a capacity reduction.

For these considerations, $LiFePO_4$ batteries are not well suited to work at low temperatures. By observing the previous functions and graphs, at first glance, it would seem that the battery works better around 50°C, i.e. at high temperatures, since the internal resistance is lower. Nevertheless, it is only a transient condition. In fact, after few cycles, the internal resistance begins to increase, consequently it is cause of an irreversible loss of capacity and loss of efficiency during the discharge and charge processes. Therefore, in conclusion high temperatures are very harmful to battery life. Figure 17 shows that higher is the ambient temperature faster the internal resistance increases and then the battery ages early.

By analysing data and curves in Figures 16 and 17, it is possible to conclude that to assure the best performances of the examined battery technology, it should never operate out of a specific temperature range, which has been experimentally estimated to be in the range from 20 °C to 30 °C. This ambient temperature interval assures good working conditions for $LiFePO_4$ batteries. The optimal trade-off between instantaneous performances and lifetime extension has been obtained with a

temperature value around 27°C.

VI. VALIDATION

To validate the model, additional discharge/charge tests have been performed on new batteries at intermediate ambient temperature values: 12 °C and 38 °C. The trend of the measured voltage values at the battery terminals has been compared with the values estimated by the model.

The V_{batt} values estimated by the model have been computed by carrying out simulations in *PSPICE environment*. The circuital model in Figure 2 has been stimulated by using the same current profiles used in the previous tests. The overall computational complexity is equal to the complexity of the *SPICE* algorithm, see [31] for further reference.

A measure of the model accuracy is given by the evaluation of the relative error. Its mean value is below 0.25%, whereas its peak value never exceeds 7%. As an example, Figure 18(a) reports the comparison between the V_{batt} values estimated by the model and the experimentally measured V_{batt} values. Figure 18(b) reports the relative error obtained during the discharge process at 12°C with an initial *SoC* of 50%. In this case study, the medium error is equal to 0.228% and the peak error obtained during the fast transients is equal to 6.9%.

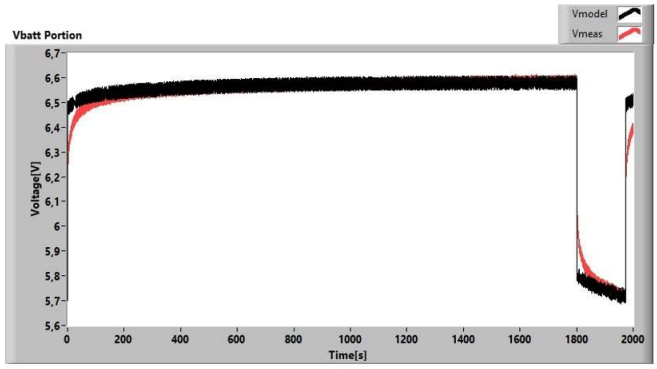

(a) V_{batt} estimated by the model vs V_{batt} measured.

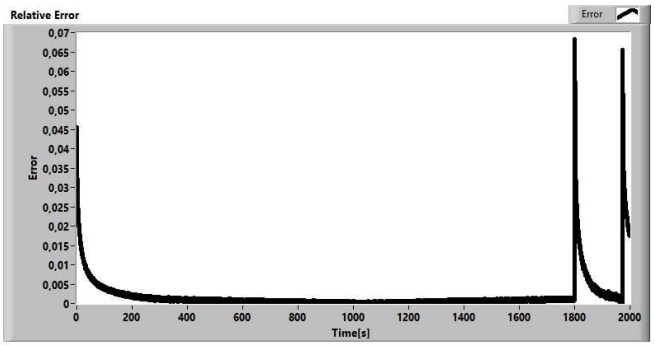

(b) Relative Error.

Fig. 18. Discharge Process: V_{batt} estimated by the model vs V_{batt} measured for T=12°C, SoC=50%.

Figure 19(a) reports the comparison between the V_{batt} values estimated by the model and the experimentally measured V_{batt} values. Figure 19(b) shows the relative error for a charge process at 12°C with an initial *SoC* of 27%.

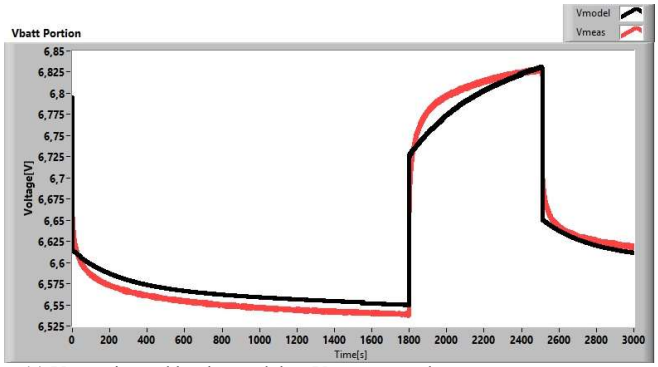

(a) V_{batt} estimated by the model vs V_{batt} measured.

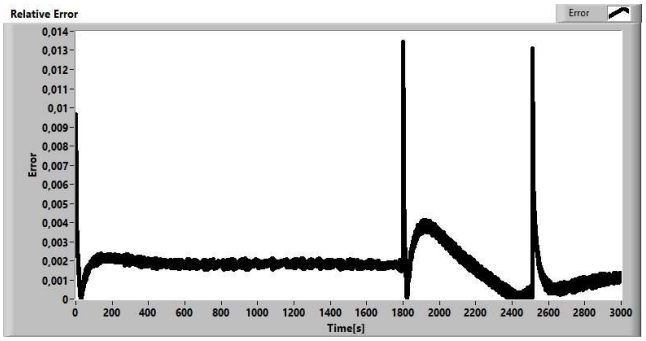

(b) Relative Error.

Fig. 19. Charge Process: V_{batt} estimated by the model vs V_{batt} measured for T=12°C, SoC=27%.

In this case study, the medium error is below 0.174% and the peak error obtained during the fast transients is equal to 1.36%.

A comparison in terms of mean relative error ($\overline{er}$[%]) and maximum relative error (er_{max}[%]) between the above proposed model and the single RC group thermal models described in [29] and [30] is reported in Table II.

TABLE II
RELATIVE ERROR OF THE MODELS

	$\overline{er}$[%] ≤	er_{max}[%] ≤
Proposed Model	0.25	6.9
Dynamic Thevenin Model [29]	1.9	4.8
Temperature dependent RC Model [30]	1	7.9

VII. CONCLUSION

In this paper, an innovative approach to characterize the thermal effects on energy storage systems has been proposed. The present study aims to prove the effectiveness and importance to use sensing systems to monitor the working temperature of battery packs used in automotive applications. For this purpose, an innovative runtime circuital model has been developed to characterize the LiFePO4 battery working conditions during the charge and discharge processes. The model has been characterized in the "Laboratorio RENEW-MEL" laboratory by means of tests performed on three different sets of $LiFePO_4$ batteries. At this moment, this battery technology is widely spread in the automotive market. Three different ambient temperature set points have been chosen for

the tests: 0 °C, 25 °C and 50 °C. A climatic chamber has been used to simulate these three thermal working conditions. Once the tests have been completed, the experimental results have been analysed in the time and frequency domains in order to get the parameters of the capacitance-resistance model of the tested battery technology. For each parameter, it has been estimated the mathematical equation describing the dependence on temperature, state of charge, state of health and number of cells. A non-linear interpolation technique has been used to fit each equation and graph to the data points. The trends of the internal resistance obtained in the several charge/discharge cycles have been analysed and compared. The present study has allowed us to highlight the significance to consider the working temperature as an indicator of battery ageing. This has entailed the identification of an ideal working temperature range for the battery technology under test in order to optimize the battery performances over time in terms of energy efficiency and extension of useful life. A further comparison with analogous works reported in literature has highlighted the good accuracy of the proposed model in terms of mean relative error.

REFERENCES

[1] Tim Williams. “The Circuit Designer Companion”. Elsevier Newnes, second edition, 2005.

[2] G. Li, J. Wu, J. Li, T. Ye, R. Morello. “Battery Status Sensing Software-Defined Multicast for V2G Regulation in Smart Grid”, in Sensors Journal IEEE, Vol. 17, no. 23, pp. 7838-7848, 2017.

[3] Zheng Liu, Rosario Morello, Wei Wu, Experiments on Battery Capacity Estimation, 2015 IEEE International Instrumentation and Measurement Technology Conference (I^2MTC 2015), May 11-14, 2015, Pisa, Italy, ISSN: 1091-5281, pp. 863-868, 2015.

[4] F.A. Amoroso, G. Cappuccino. “Advantages of efficiency-aware smart charging strategies for PEVs”, in Energy Conversion and Management, Vol. 54, no. 1, pp. 1-6, 2012.

[5] S Piller, M Perrin, A Jossen. “Methods for state-of-charge determination and their applications”, in Journal of Power Sources, Vol. 96, no.1, pp. 113-120, 2001.

[6] SM Rezvanizaniani, Z Liu, Y Chen, J Lee. “Review and recent advances in battery health monitoring and prognostics technologies for electric vehicle (EV) safety and mobility”, in Journal of Power Sources, Vol. 256, no. 15, pp. 111-124, 2014.

[7] M.R. Jongerden and B.R. Haverkort. “Battery modeling”, in CTIT Technical Report Series, no. TR-CTIT-08-01, 2008.

[8] Yakup S. Ozkazanc, Koray Kutluay, Yigit Cadirci and Isik Cadirci. “A new online state-of-charge estimation and monitoring system for sealed lead-acid batteries in telecommunication power supplies”, in IEEE Transactions on Industrial Electronics, Vol. 52, no. 5, pp. 1315-1327, 2005.

[9] Yukihiro Toyota, Takayuki Torikai, Takaaki Takesue and Kazushi Nakano. “Research and development of the model-based battery state of charge indicator”, in Proceedings of the 1992 International Conference on Industrial Electronics, Control, Instrumentation and Automation, 1992.

[10] S. Drouilhet and B.L. Johnson. “A battery life prediction method for hybrid power applications”, NREL/CP-440-21978, 1997.

[11] O. Kanoun, U Troltzsch and H. Trankler. “Characterizing aging effects of lithium ion batteries by impedance spectroscopy”, in Electrochimica Acta, Vol. 51, no. 8-9, pp. 1664-1672, 2006.

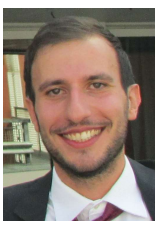

[12] Ralph E. White, Gerardine G. Botte, Venkat R. Subramanian. “Mathematical modeling of secondary lithium batteries”, in Electrochimica Acta Vol. 45 no. 15-16, pp. 2595-2609, 1999.

[13] Ralph E. White, Long Cai. “Mathematical modeling of a lithium ion battery with thermal effects in comsol inc. multiphysics (mp) software”, in Journal of Power Sources, Vol. 196, no.14, pp. 5985-5989, 2011.

[14] Dirk Uwe Sauer, Alexander Farmann, Wladislaw Waag. “Adaptive approach for on-board impedance parameters and voltage estimation of lithium-ion batteries in electric vehicles”, in Journal of Power Sources, Vol. 299, pp. 176-188, 2015.

[15] Dirk Uwe Sauer, Wladislaw Waag, Christian Fleischer. “On-line estimation of lithium-ion battery impedance parameters using a novel varied-parameters approach”, in Journal of Power Sources, Vol. 237, pp. 260-269, 2013.

[16] Hans-Martin Heyn, Dirk Uwe Sauer, Christian Fleischer, Wladislaw Waag. “On-line adaptive battery impedance parameter and state estimation considering physical principles in reduced order equivalent circuit battery models: Part 2. parameter and state estimation”, in Journal of Power Sources, Vol. 262, pp. 457-482, 2014.

[17] D Gallo, C Landi, M Luiso, R Morello. “Optimization of experimental model parameter identification for energy storage systems”, in Energies, Vol. 6, no. 9, pp. 4572-4590, 2013.

[18] C. Chiasserini and R. Rao. “Energy efficient battery management”, in IEEE Journal on Selected Areas in Communications , Vol. 19, no. 7, pp. 1235-1245, 2001.

[19] A. Kumar, V. Rao, G. Singhal and N. Navet. “Battery model for embedded systems”, in Proceedings of the 18th International Conference on VLSI Design held jointly with 4th International Conference on Embedded Systems Design (VLSID'05), pp. 105-110, 2005.

[20] Hengjuan Cui, Wei Liang, Michael Pecht, Qiang Miao, Lei Xie. “Remaining useful life prediction of lithium-ion battery with unscented particle filter technique”, in Microelectronics Reliability, Vol. 53, no. 8, pp. 805-810, 2013.

[21] Bhaskar Saha and Kai Goebel. “Modeling li-ion battery capacity depletion in a particle filtering framework”, in Proceedings of the Annual Conference of the Prognostics and Health Management Society, 2009.

[22] C.M. Shepherd. “Design of primary and secondary ceils”, in J. Electrochem. Soc., Vol. 112, no. 8, pp. 657-664, 1965.

[23] D. Rakhmatov and S. Vrudhula. “An analytical high-level battery model for use in energy management of portable electronic systems”, in ICCAD '01 Proceedings of the 2001 IEEE/ACM international conference on Computer-aided design, pp. 488-493, 2001.

[24] G.A. Rincon-Mora, Min Chen. “Accurate electrical battery model capable of predicting runtime and i-v performance”, in IEEE Transactions on Energy Conversion, Vol. 21, no. 2, pp. 504-511, 2006.

[25] D. Robertson, M. Valvo, F. E. Wicks and S. Rudin. “Development and application of an improved equivalent circuit model of a lead acid battery”, in Proc. Energy Conversion Engineering Conf, Vol. 2, pp. 1159-1163, 1996.

[26] H He, R Xiong, J Fan. “Evaluation of Lithium-Ion Battery Equivalent Circuit Models for State of Charge Estimation by an Experimental Approach”, in Energies, Vol. 4, no. 4, pp. 582-598, 2011.

[27] Gianluca Aurilio, Daniele Gallo. “Tecniche di previsione, gestione e monitoraggio online dello stato interno di una batteria per applicazioni smart-grid”, 2015.

[28] C. Landi, M. Luiso, A. Rosano, M. Landi, V. Paciello, G. Aurilio, D. Gallo. “A battery equivalent-circuit model and an advanced technique for parameter estimation”. In 2015 IEEE International Instrumentation and Measurement Technology Conference (I2MTC) Proceedings, pp. 1705-1710, 2015.

[29] M. Malik, M. Mathew, I. Dincer, M.A. Rosen, J. McGrory, M. Fowler. “Experimental investigation and thermal modelling of a series connected LiFePO4 battery pack”. In International Journal of Thermal Sciences, Vol.132, pp. 466-477, 2018.

[30] Chin, C.S.; Gao, Z.; Chiew, J.H.K.; Zhang, C. “Nonlinear Temperature-Dependent State Model of Cylindrical $LiFePO_4$ Battery for Open-Circuit Voltage, Terminal Voltage and State-of-Charge Estimation with Extended Kalman Filter”. In Energies, Vol. 11, no. 9, pp. 2467-2495.

[31] Qilin Zhang, Habti Abeida, Ming Xue, William Rowe, and Jian L. “Fast implementation of sparse iterative covariance-based estimation for source localization”. In The Journal of the Acoustical Society of America, Vol. 131, no.2, pp.1249-1259.

Filippo Ruffa was born in Bologna, BO, Italy in 1990. He received the B.S. degree and the M.S. degree (magna cum laude) in electronic engineering from the University of Calabria, in 2012 and 2015. He is a Ph.D. Student in information engineering at University Mediterranea of Reggio Calabria since 2015. He attended to two Ph.D. schools and successfully passed the final exam: the “Italo Gorini 2017” in Catania, and the “Italo Gorini 2018” at CERN in Geneva.

His main research interests include modeling and characterization of energy storage systems, energy management, smart measurement systems, sensor networks, biomedical applications.

He is a junior member of the Italian Group of Electric and Electronic Measurements since 2015.

Claudio De Capua (M'99) received the M.S. and the Ph.D. degrees in Electrical Engineering from the University of Naples "Federico II", Naples, Italy. Since 2012, he is Full Professor of Electrical and Electronic Measurements at the Department of Information Engineering, Infrastructure and Sustainable Energy, University "Mediterranea" of Reggio Calabria. His current research includes the design, realization and metrological performance improvement of the automatic measurement systems; web sensors and sensor data fusion; biomedical instrumentation; techniques for remote didactic laboratory; measurement uncertainty analysis; problems of electromagnetic compatibility in measurements.
Prof. De Capua is member of the Italian Group of Electrical and Electronic Measurements (GMEE).

Rosario Morello (M'03) was born in Reggio Calabria, Italy, in 1978. He received the M.Sc. Degree (cum laude) in Electronic Engineering and the Ph.D. Degree in Electrical and Automation Engineering from the University "Mediterranea" of Reggio Calabria, Italy, in 2002 and 2006, respectively. Since 2005, he has been Postdoctoral Researcher of Electrical and Electronic Measurements at the Department of Information Engineering, Infrastructure and Sustainable Energy of the same University. At the present he is an Assistant Professor and is Scientific Director of the *Advanced Thermography Center* at University Mediterranea. His main research interests include the design and characterization of distributed and intelligent measurement systems, advanced thermography, wireless sensor network, environmental monitoring, decision-making problems and measurement uncertainty, process quality assurance, instrumentation reliability and calibration, energy, smart grids, battery testing, biomedical applications and statistical signal processing, non-invasive systems, biotechnologies and measurement, instrumentation and methodologies related to Healthcare. Prof. Morello is a member of IEEE and serves as AE for the IEEE Sensors J.

Zheng Liu (M'02–SM'06) received the Doctorate degree in engineering from Kyoto University, Kyoto, Japan, in 2000, and the Ph.D. degree from the University of Ottawa, Canada, in 2007. From 2000 to 2001, he was a Research Fellow with Nanyang Technological University, Singapore. He then joined the Institute for Aerospace Research (IAR), National Research Council Canada, Ottawa, ON, Canada, as a Governmental Laboratory Visiting Fellow nominated by NSERC. After being with IAR for 5 years, he transferred to the NRC Institute for Research in Construction, where he was a Research Officer. From 2012 to 2015, he worked as a full Professor with Toyota Technological Institute, Nagoya, Japan. He is now with the School of Engineering at the University of British Columbia (Okanagan). His research interests include image/data fusion, computer vision, pattern recognition, senor/sensor network, condition-based maintenance, and non-destructive inspection and evaluation. He is a senior member of IEEE and a member of SPIE. He is chairing the IEEE IMS technical committee on "industrial inspection" (TC-36). He holds a Professional Engineer license in British Columbia and Ontario. Dr. Liu serves on the editorial board for journals: the IEEE Transactions on Instrumentation and Measurement, IEEE Instrumentation and Measurement Magazine, Information Fusion, Machine Vision and Applications, and Intelligent Industrial Systems.